Journal of Power Sources 267 (2014) 269–279

Contents lists available at ScienceDirect

Journal of Power Sources

journal homepage: www.elsevier.com/locate/jpowsour

Structural, thermomechanical and electrical properties of new $(1-x)Ce_{0.8}Nd_{0.2}O_{2-\delta}$–$xBaCe_{0.8}Nd_{0.2}O_{3-\delta}$ composites

D. Medvedev [a], E. Pikalova [a, b], A. Demin [a, 1], A. Podias [c], I. Korzun [a], B. Antonov [a], P. Tsiakaras [a, c, *]

[a] Institute of High Temperature Electrochemistry, 620990 Yekaterinburg, Russia
[b] Department of Environmental Economics, Ural Federal University, 620002 Yekaterinburg, Russia
[c] Department of Mechanical Engineering, School of Engineering, University of Thessaly, Pedion Areos, 383 34 Volos, Greece

HIGHLIGHTS

- The total conductivity of $(1-x)Ce_{0.8}Nd_{0.2}O_{2-\delta}$–$xBaCe_{0.8}Nd_{0.2}O_{3-\delta}$ composites in wet air is lower than that of the basic oxides.
- Their conductivity degradation is not more than 15% for 200 h of redox-cycles at 900 °C.
- Their stability in CO_2- and H_2O-containing atmospheres may render them as potential candidates for IT-SOFCs.

GRAPHICAL ABSTRACT

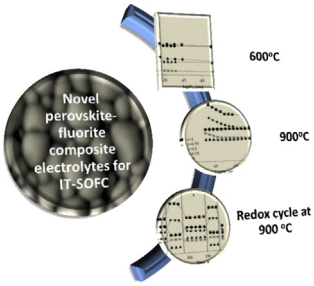

ARTICLE INFO

Article history:
Received 4 September 2013
Received in revised form
1 May 2014
Accepted 13 May 2014
Available online 21 May 2014

Keywords:
Composite electrolytes
Doped CeO_2
Doped $BaCeO_3$
Ionic conductivity
Thermal expansion
IT-SOFC

ABSTRACT

In this work composite $(1-x)Ce_{0.8}Nd_{0.2}O_{2-\delta}$–$xBaCe_{0.8}Nd_{0.2}O_{3-\delta}$ ceramics were prepared via the one-step citrate-nitrate combustion procedure, and characterised by TG-DSC, XRD analysis, and SEM. Their transport properties were investigated across various temperatures (600–900 °C) and oxygen partial pressures (10^{-23}–0.21 atm).

The XRD data reveals an occurrence of single-phase oxides at $x = 0, 1$ and two phases with perovskite and fluorite structure at $x = 0.25, 0.5, 0.75$ in powders calcined at 1100 °C. Dense ceramic samples (93–95%) were sintered in air at 1500 °C for 3 h. The concentration dependence of the mean grain size is characterized by local minimum at $x = 0.5$, while that of total conductivity exhibited a similar behavior; its minimal value was registered in the sample with the most extended specific grain surface. It was found that the electronic contribution to the total conductivity of the composites is reduced as compared to that of the basic $Ce_{0.8}Nd_{0.2}O_{2-\delta}$ and $BaCe_{0.8}Nd_{0.2}O_{3-\delta}$ materials. This leads to a better stability in the long-term redox-cycles in comparison with the basic oxides.

Additionally, the conductivity in $Ce_{0.8}Nd_{0.2}O_{2-\delta}$ decreases by 85%, whereas the conductivity of $BaCe_{0.8}Nd_{0.2}O_{3-\delta}$ decreases by 30% after 2 redox-cycles for 200 h at 900 °C. The resulting conductivity degradation of the $(1-x)Ce_{0.8}Nd_{0.2}O_{2-\delta}$–$xBaCe_{0.8}Nd_{0.2}O_{3-\delta}$ composite is no more than 15%.

* Corresponding author. Department of Mechanical Engineering, School of Engineering, University of Thessaly, Pedion Areos, 383 34 Volos, Greece. Tel.: +30 24210 74065; fax: +30 24210 74050.
E-mail addresses: a.demin@ihte.uran.ru (A. Demin), tsiak@mie.uth.gr (P. Tsiakaras).
[1] Tel.: +7 343 3745431; fax: +7 343 3745992.

http://dx.doi.org/10.1016/j.jpowsour.2014.05.070
0378-7753/

1. Introduction

Currently, most research in the development of electrolyte materials for solid oxide fuel cells (SOFCs) is focused on the design and development of new oxide systems that have high ionic conductivity and stability under working conditions [1–4]. Among the most investigated materials, cerium oxide and barium cerate based materials are suitable for use in intermediate temperature SOFCs (IT-SOFCs), because of their shared properties of high ionic conductivity [1–6]. However, there are still certain significant drawbacks hindering the use of these materials in SOFCs. These include low stability in a reducing atmosphere, a characteristic which is more pronounced in cerium oxide [1–4], and the chemical destruction of materials based on barium cerate in CO_2-containing atmospheres [5,6]. At present, optimization of the functional properties of these materials is achieved through two principal methodologies. The first entails the doping of these oxide systems using different additives, which results in: better sinterability, an increase in electrical conductivity, and structural stability in reducing and CO_2 or H_2O rich atmospheres [1–6]. Another possible way to overcome the problems associated with the use of materials based on cerium oxide and barium cerate is through the creation of composite materials based on these substances [7–13]. There are some published investigations of such composite systems as $(1-x)Ce_{0.8}Gd_{0.2}O_{2-\delta}$–$xBaCe_{0.8}Gd_{0.2}O_{3-\delta}$ ($0 \le x \le 0.4$) [7,8], $(1-x)Ce_{0.8}Sm_{0.2}O_{2-\delta}$–$xBaCe_{0.8}Sm_{0.2}O_{3-\delta}$ ($x = 0$, 0.3, 0.36, 0.5, 0.7, 1) [9,12], $0.5Ce_{0.8}Y_{0.2}O_{2-\delta}$–$0.5BaCe_{0.8}Gd_{0.2}O_{3-\delta}$ [10], and $(100-x)Ce_{0.8}Y_{0.2}O_{2-\delta}$–$xBaCe_{0.7}Zr_{0.1}Y_{0.2}O_{3-\delta}$ ($x = 20$, 30, 50 and 70 wt.%) [11], where the cause–effect relationship between chemical content, structure and electrical/electrochemical properties of the materials were elucidated. Preliminary studies have shown: i) extended electrolytic area of composite electrolytes due to a decrease in the electronic conductivity at the low pO_2 by blocking with barium cerate phase, and vice versa, a reduction of the hole conductivity in oxidizing conditions caused by the blocking with ceria phase [9,12]; ii) enhanced stability of ceramics at low and high pO_2 values and in CO_2-, H_2O-containing atmospheres [12]; and iii) better electrochemical characteristics (open circuit voltage, power density) of unit SOFCs in comparison with those obtained for CeO_2- and $BaCeO_3$-based SOFCs [7–9,13].

Nd-doped CeO_2 and $BaCeO_3$ ceramics with advanced electrical properties widely investigated and presented in literature [14–18] were chosen in the present work to prepare similar composite systems. The series of studies we carried out were focused on the synthesis and evaluation of prepared system $(1-x)Ce_{0.8}Nd_{0.2}O_{2-\delta}$–$xBaCe_{0.8}Nd_{0.2}O_{3-\delta}$ ($x = 0$, 0.25, 0.5, 0.75, 1) and systematic study of their thermo-mechanical, electrical and electrochemical properties.

2. Experimental

$Ba(NO_3)_2$ (purity 99.95%), $Ce(NO_3)_3\cdot 6H_2O$ (purity 99.9%) and $Nd(NO_3)_3\cdot 6H_2O$ (purity 99.9%) were used as starting materials. The compositions of $(1-x)Ce_{0.8}Nd_{0.2}O_{2-\delta}$–$xBaCe_{0.8}Nd_{0.2}O_{3-\delta}$ ($x = 0$, 0.25, 0.5, 0.75, 1) were obtained by employing the citrate-nitrate method described in detail in the work of Chen et al. [19]. To intensify the combustion process the amount of citric acid was taken with an excess of 30 wt.% relative to stoichiometric value (φ) calculated from the following reaction [12,20]:

$$x\mathrm{Ba(NO_3)_2} + 0.8\mathrm{Ce(NO_3)_3\cdot 6H_2O} + 0.2\mathrm{Nd(NO_3)_3\cdot 6H_2O} + 1.3\varphi\mathrm{C_6H_8O_7} \rightarrow (1-\mathrm{x})\mathrm{Ce_{0.8}Nd_{0.2}O_{1.9}} - \mathrm{xBaCe_{0.8}Nd_{0.2}O_{2.9}} + 7.8\varphi\mathrm{CO_2} + (6+5.2\varphi)\mathrm{H_2O} + (2x+3)/2\mathrm{N_2} \quad (1)$$

The thermogravimetric (TG) and thermochemical (DSC) studies of the as-combusted powders were carried out by synchronous thermal analyzer STA 449C Jupiter® (NETZSCH, Germany) in an air atmosphere, in a temperature range of 20–1350 °C.

The as-combusted powders were annealed at 600 °C for 5 h with subsequent calcination at 1100 °C for 3 h, to remove undecomposed organic particles and nitrates, and to obtain corresponding oxide components. The powders were examined by X-ray powder diffraction analysis (XRD, D/MAX–2200 RIGAKU) in the range of $15° \le 2\theta \le 85°$. The ceramic samples for electrical and thermal investigations $(1-x)Ce_{0.8}Nd_{0.2}O_{2-\delta}$–$xBaCe_{0.8}Nd_{0.2}O_{3-\delta}$ ($x = 0$, 0.25, 0.5, 0.75 and 1) were sintered at 1500 °C for 3 h in air with a heating/cooling rate of 2 °C min^{-1}. The surface morphology of the sintered samples before and after long-term conductivity measurements was investigated via scanning electron microscopy (SEM, JSM-5900 LV). The density of the sintered samples was measured employing both the Archimedes principle with kerosene, and calculations from the weights and dimensions of the specimens. It was found that both methods of obtaining the density gave almost the same value of about 93–95%.

Electrical conductivity measurements of the samples were carried out employing the four-point probe dc technique in different atmospheres. The specimens were installed in a tube made of ZrO_2-based electrolyte. Platinum paste stripes deposited on the inner and outer surface of the yttria-stabilized zirconia (YSZ) tube connected by platinum wires were used as the electrochemical oxygen pump and the oxygen sensor. The atmospheres with various oxygen partial pressures inside the tube were also created by means of oxygen pumping and registered by the sensor. Temperature and oxygen partial pressure were automatically varied by means of a microprocessor system (ZIRKONIA-318 [21]) in the range of 550–900 °C and 10^{-23}–0.1 atm, respectively. Four Pt electrodes were deposited on the samples' surface and connected by Pt wire. One pair was used to apply voltage and the second pair to register the current along the samples. All measurements were made and registered automatically. The degradation of materials, with respect to electrical conductivity, was investigated at 900 °C for 200 h under dynamically changing atmospheric conditions (redox-cycles).

Thermal and chemical expansion of the samples was measured by Tesatronic TT-80 dilatometer in air during heating from room temperature to 900 °C with a rate of 3 °C min^{-1}.

3. Results and discussions

3.1. Synthesis

TG-DSC was carried out in air for the as-combusted precursors of all the samples. As an example, Fig. 1 depicts the results for the $BaCe_{0.8}Nd_{0.2}O_{3-\delta}$. The graph shows that there is a gradual decrease in the mass of powders in the range 100–300 °C, 300–500 °C, 500–700 °C and 750–1160 °C by 0.5, 1.5, 2.2 and 10 wt.%, respectively. According to the analysis of the off-gases, this mass change corresponds to desorption from the surface of the powder-free or crystal-bound water, CO_2 (which is the product of the oxidation of the fuel), and nitrogen-containing components (mainly, NO). The last remarkable change in mass is connected with the decomposition of $BaCO_3$, an intermediate phase in the synthesis process [12,20], which results in the formation of the corresponding oxide. At the temperatures above 1150 °C no change in mass was registered. A similar tendency was observed for the other powders of $(1-x)Ce_{0.8}Nd_{0.2}O_{2-\delta}$–$xBaCe_{0.8}Nd_{0.2}O_{3-\delta}$ (Fig. 2a). It should be noted that the mass change of $Ce_{0.8}Nd_{0.2}O_{2-\delta}$ powder in the temperature range 25–1350 °C was a minimal one (no more than

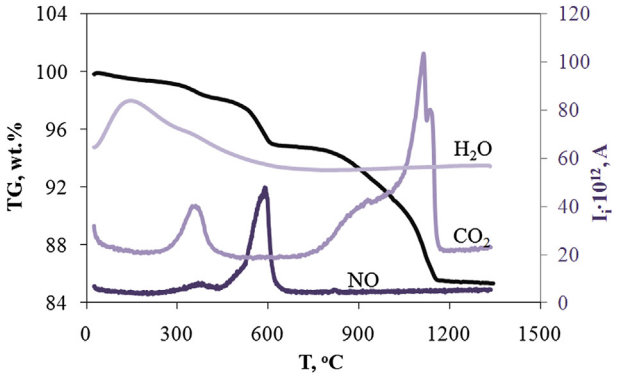

Fig. 1. TG and ion current response (I_i) curves of as-combusted $BaCe_{0.8}Nd_{0.2}O_{3-\delta}$ powder.

5 wt.%). This is due to the fact that the process of fuel oxidation by reaction (1) is almost complete in this case, and a small change in mass appears only because of the burning of C-containing residues.

The mass change measurements concur with DSC analysis data (Fig. 2b). There is a small endothermic peak in the low temperature range that corresponds to the water desorption from the surface of the powders. An exothermic effect followed by an endothermic peak registered near 600 °C for perovskite-rich powders are connected with the reduction of nitrate-groups to nitrogen-containing gaseous components (N_2, N_2O, NO_2, NO, with a predominance of the latter) followed by their removal [22]. An additional endothermic effect was also found near 830–840°C for the composite materials $(1-x)Ce_{0.8}Nd_{0.2}O_{2-\delta}$–$xBaCe_{0.8}Nd_{0.2}O_{3-\delta}$ at $x = 0.5$, 0.75, and 1. It corresponds to the phase $\gamma \rightarrow \beta$ transition of $BaCO_3$ [12]. With a further increase in temperature DSC curves for these compounds attain a complex shape because of the parallel processes of decomposition of barium carbonate and the formation of the final product.

Since the TG-DSC analysis was performed in a dynamic regime, a slightly decreased temperature of calcinations of 1100 °C for 3 h was chosen later. In Fig. 3 the XRD data of the calcined $(1-x)Ce_{0.8}Nd_{0.2}O_{2-\delta}$–$xBaCe_{0.8}Nd_{0.2}O_{3-\delta}$ powders are presented. There are only X-ray reflections related to the phases of fluorite (Fm3m) and perovskite (orthorhombic distortion, Pmcn) for $Ce_{0.8}Nd_{0.2}O_{2-\delta}$ and $BaCe_{0.8}Nd_{0.2}O_{3-\delta}$ materials, respectively. According to XRD the composite materials are two-phase and demonstrate the same reflexes as the basic phases without their interaction. The results of X-ray refinement are presented in Table 1. It can be seen that with an increase in perovskite phase content the lattice parameters of an orthorhombic structure remain virtually unchanged, while the parameters of a cubic structure grow. An increase in unit cells for CeO_2-based materials of $(1-x)Ce_{0.8}Gd_{0.2}O_{2-\delta}$–$xBaCe_{0.8}Gd_{0.2}O_{3-\delta}$ ($0 \le x \le 0.4$) was also observed in Ref. [8] showing the tendency of increasing Gd-content in fluorite phase correspondingly specified value. The same tendency probably appears in Nd-doped CeO_2–$BaCeO_3$ system.

3.2. Microstructure

The microstructure of the ceramic samples sintered at 1500 °C for 3 h was characterized by SEM and presented in Fig. 4. It can be seen that the pellets have a high density, with very low porosity, which is in accordance with the relative densities of the $(1-x)Ce_{0.8}Nd_{0.2}O_{2-\delta}$–$xBaCe_{0.8}Nd_{0.2}O_{3-\delta}$ ceramic samples measured by hydrostatic weighing in kerosene (Table 2). Moreover, no detectable traces of impurity phases or segregations at the grain boundaries were found in any of the samples studied.

For a qualitative estimation of the surface microstructure of the sintered ceramic samples, the size of each grain was determined and histograms of the particle size distribution were obtained (Fig. 4). The mean grain size of composite materials did not differ significantly and varied from 1.2 to 1.7 μm (Table 2). In contrast, for the basic materials of $Ce_{0.8}Nd_{0.2}O_{2-\delta}$ and $BaCe_{0.8}Nd_{0.2}O_{3-\delta}$ significant grain growth up to 3.7 and 7.8 μm was observed, respectively. In the case of single-phase materials grain growth during the sintering process is understandably more intense due to the large contact surface area of one type of powder particle. In the case of composite (two-phase) materials, grain growth is limited by the diffusion difficulties associated with the presence of particles of another phase.

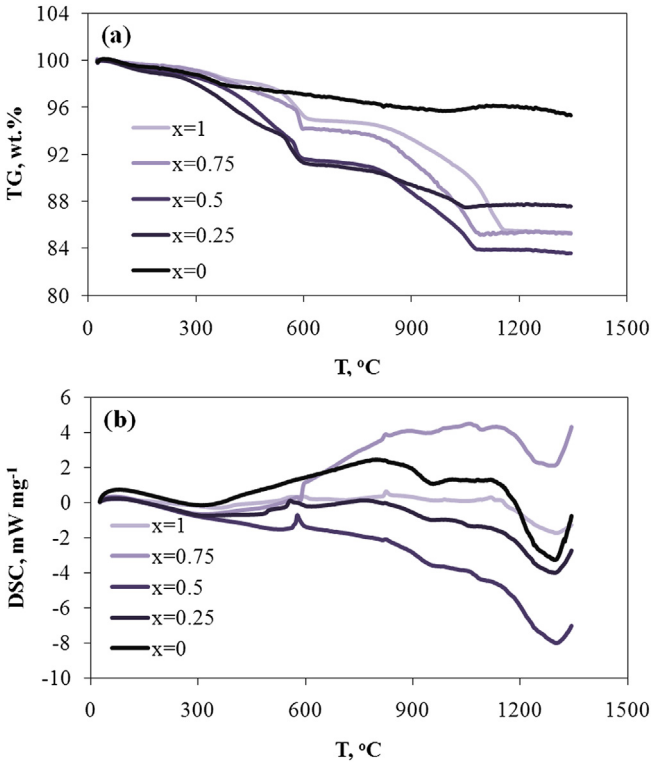

Fig. 2. (a) TG and (b) DSC curves of the as-combusted $(1-x)Ce_{0.8}Nd_{0.2}O_{2-\delta}$–$xBaCe_{0.8}Nd_{0.2}O_{3-\delta}$ powders.

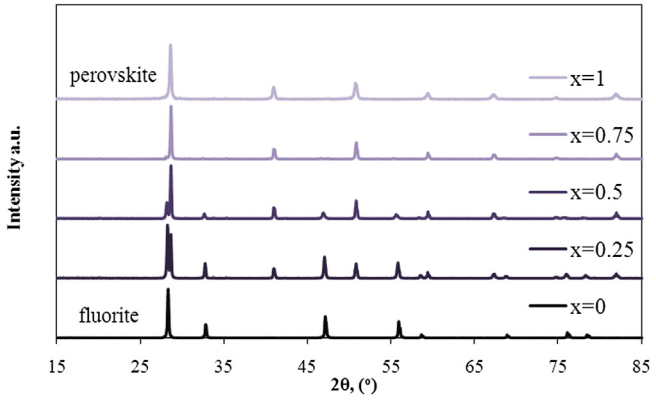

Fig. 3. The XRD diffraction patterns for $(1-x)Ce_{0.8}Nd_{0.2}O_{2-\delta}$–$xBaCe_{0.8}Nd_{0.2}O_{3-\delta}$ samples calcined at 1100 °C for 3 h.

Table 1
The structure properties of $(1-x)Ce_{0.8}Nd_{0.2}O_{2-\delta}$–$xBaCe_{0.8}Nd_{0.2}O_{3-\delta}$ powders calcined at 1100 °C for 3 h. F – fluorite phase (sp.gr. Fm3m), P – perovskite phase (sp.gr. Pmcn).

x	Phase individuality	Unit cell parameters of fluorite phase		Unit cell parameters of perovskite phase			
		a, Å	V, Å^3	a, Å	b, Å	c, Å	V, Å^3
0	F	5.4462(3)	161.55(2)				
0.25	F + P	5.4562(3)	162.43(2)	8.7731(9)	6.2313(4)	6.2143(4)	339.73(5)
0.5	F + P	5.4755(7)	163.05(3)	8.7770(5)	6.2334(3)	6.2148(5)	340.02(4)
0.75	P+ trace of F			8.774(1)	6.2298(6)	6.2206(4)	340.01(6)
1	P			8.779(2)	6.230(1)	6.2246(8)	340.4(1)

3.3. Electrical conductivity

The effect of temperature on the total conductivity of $(1-x)Ce_{0.8}Nd_{0.2}O_{2-\delta}$–$xBaCe_{0.8}Nd_{0.2}O_{3-\delta}$ samples measured in a wet air atmosphere is depicted in Fig. 5. The temperature dependence of the total conductivity of both fluorite and perovskite systems can be described with semiconducting type conductivity. For $BaCe_{0.8}Nd_{0.2}O_{3-\delta}$ the activation energy (E_a) is equal to 0.52 ± 0.03 eV in the range of 550–750 °C and 0.54 ± 0.03 eV in the range of 750–900 °C, whereas for $Ce_{0.8}Nd_{0.2}O_{2-\delta}$ it is equal to 0.79 ± 0.04 eV

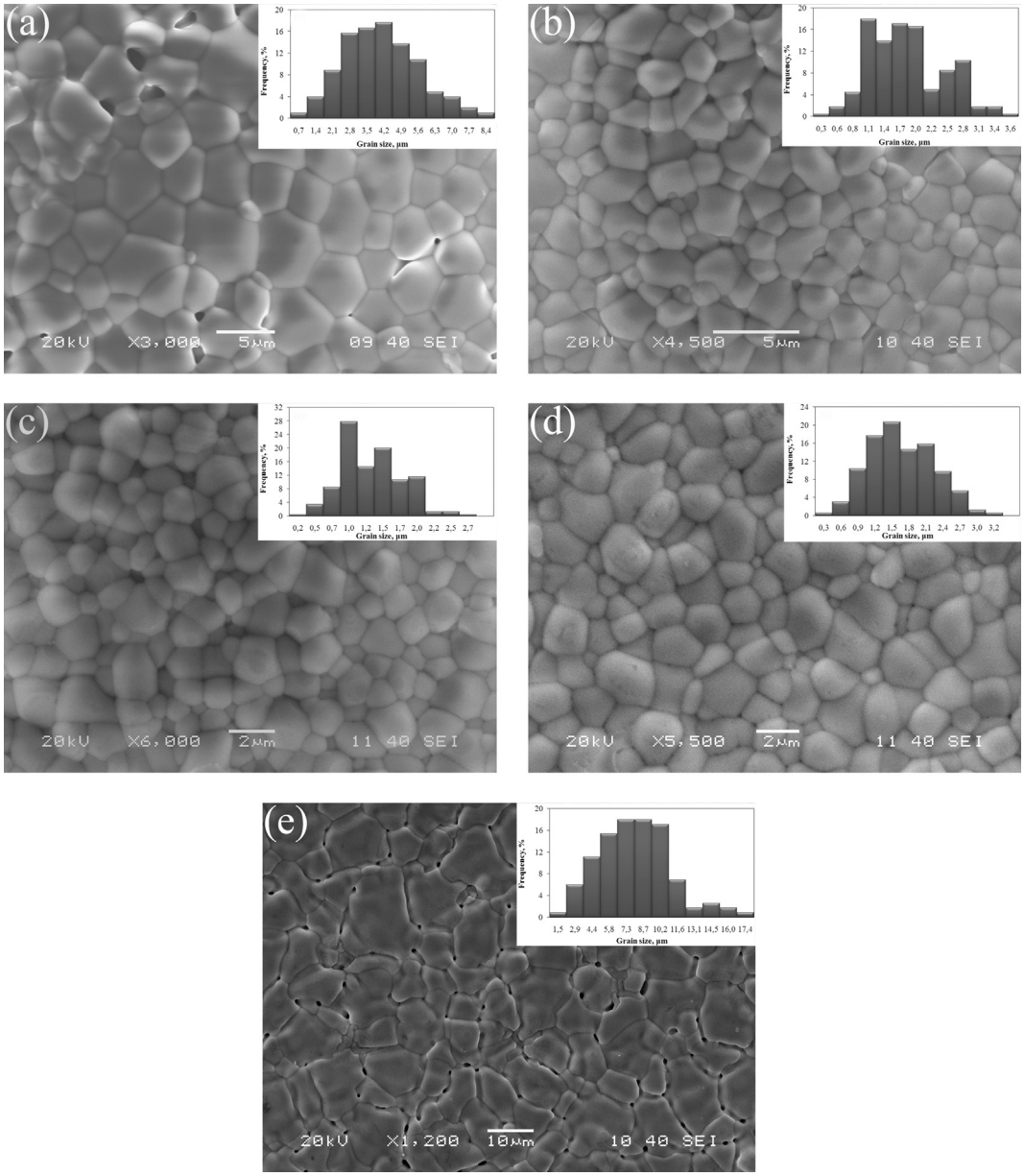

Fig. 4. The SEM micrographs and grain size distribution histograms for $(1-x)Ce_{0.8}Nd_{0.2}O_{2-\delta}$–$xBaCe_{0.8}Nd_{0.2}O_{3-\delta}$ ceramic samples sintered at 1500 °C for 3 h: (a) $x = 0$, (b) $x = 0.25$, (c) $x = 0.5$, (d) $x = 0.75$, (e) $x = 1$.

Table 2
The structure properties of $(1-x)Ce_{0.8}Nd_{0.2}O_{2-\delta}$–$xBaCe_{0.8}Nd_{0.2}O_{3-\delta}$ ceramic samples sintered at 1500 °C.

x	Relative density, %	Mean grain size, μm
0	93.2	7.8
0.25	95.4	1.5
0.5	94.1	1.2
0.75	96.5	1.7
1	94.7	3.7

in the range of 550–750 °C and 0.75 ± 0.03 eV in the range of 750–900 °C (inset of Fig. 5), which agrees with data presented in literature [23,24]. As is known, at low temperatures in wet air, protonic conductivity prevails in $BaCeO_3$ materials [25–27]. With an increase in temperature the protonic conductivity decreases with a simultaneous increase in the oxygen ionic and p-type electronic (hole) conductivity. Since the E_a of the protonic conductivity (0.3–0.6 eV) is lower than that of the oxygen ionic (0.6–0.9 eV) and the hole conductivity (0.7–1.4 eV) [5,26,28], the result is an increase in E_a in the high temperature interval. In CeO_2-based materials, at low temperatures, the process of association of acceptor defects and free oxygen vacancies $\{Nd'_{Ce} - V^{\bullet\bullet}_O\}^{\bullet}$, $\{Nd'_{Ce} - V^{\bullet\bullet}_O - Nd'_{Ce}\}^{x}$ [7,16] appears, resulting in an increase of E_a.

Since the conductivity values of basic oxides are close to those in the literature (Fig. 5) then it can be seen that the total conductivity of composite materials in wet air is lower than it is for basic oxides. The same tendency was found in $(100-x)Ce_{0.8}Y_{0.2}O_{2-\delta}$–$xBaCe_{0.7}Zr_{0.1}Y_{0.2}O_{3-\delta}$ (x = 0, 20, 30, 50, 70 and 100 wt.%) [11], and $(1-x)Ce_{0.8}Gd_{0.2}O_{2-\delta}$–$xBaCe_{0.8}Gd_{0.2}O_{3-\delta}$ (x = 0, 0.2, 0.3 and 0.4) [7] composites. In the case of composites on a base of $Ce_{0.8}Y_{0.2}O_{2-\delta}$ and $BaCe_{0.7}Zr_{0.1}Y_{0.2}O_{3-\delta}$ the authors attribute this behavior to the appearance of low conducting phases such as Ba_2YZrO_6 and Ba_2ZrO_4 localized on the grain boundaries, which deteriorate the charge carriers' transport [11]. The decrease in total conductivity of the $Ce_{0.8}Gd_{0.2}O_{2-\delta}$ and $BaCe_{0.8}Gd_{0.2}O_{3-\delta}$ composites is connected with a contact (interfacial) resistance at the $BaCe_{0.8}Gd_{0.2}O_{3-\delta}$–$Ce_{0.8}Gd_{0.2}O_{2-\delta}$ interface [7]. Since secondary phases in composites were not registered, it is probable that the decrease in conductivity, in the case of the Nd-doped system, is connected with a high contact resistance at the boundaries between two different phases, which must necessarily lead to an increase in E_a for the total conductivity (inset of Fig. 5). The maximum value of E_a was calculated for $0.5Ce_{0.8}Nd_{0.2}O_{2-\delta}$–$0.5BaCe_{0.8}Nd_{0.2}O_{3-\delta}$ ceramic sample, which

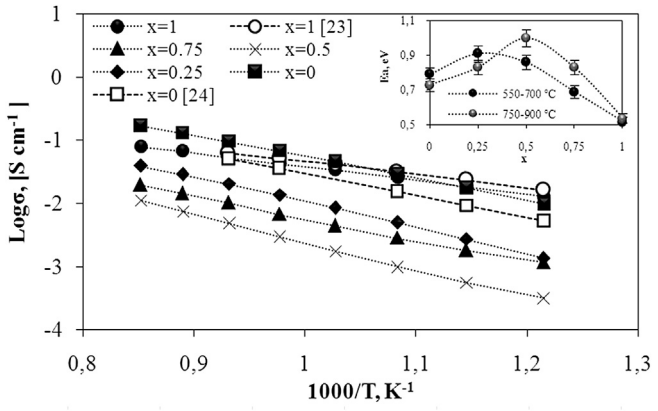

Fig. 5. Effect of temperature on total conductivity of $(1-x)Ce_{0.8}Nd_{0.2}O_{2-\delta}$–$xBaCe_{0.8}Nd_{0.2}O_{3-\delta}$ (x = 0, 0.25, 0.5, 0.75, 1) samples, in wet air atmosphere compared with literature data for basic materials [23,24]. Inset: concentration dependence of the activation energy in $(1-x)Ce_{0.8}Nd_{0.2}O_{2-\delta}$–$xBaCe_{0.8}Nd_{0.2}O_{3-\delta}$ (x = 0, 0.25, 0.5, 0.75, 1) samples in wet air.

at the same time had the lowest conductivity. The level of activation energy in the low and high temperature ranges in the composite sample with $x = 0.25$ is similar to that in $Ce_{0.8}Nd_{0.2}O_{2-\delta}$. This may indicate that the conductivity in $0.75Ce_{0.8}Nd_{0.2}O_{2-\delta}$–$0.25BaCe_{0.8}Nd_{0.2}O_{3-\delta}$ is primarily controlled by the fluorite phase. For composites with $x = 0.5$ and 0.75 transport is apparently controlled by the perovskite phase. It should be noted that, in other systems based on CeO_2–$BaCeO_3$, when increasing the perovskite phase content a gradual decrease in E_a was registered regardless of the presence of phases with poor conductivity [11] or interfacial resistance [7].

Fig. 6 shows the oxygen partial pressure dependence of the total conductivity in $(1-x)Ce_{0.8}Nd_{0.2}O_{2-\delta}$–$xBaCe_{0.8}Nd_{0.2}O_{3-\delta}$ samples at various temperatures, obtained by electrochemical pumping of oxygen from wet air. Conductivity behavior with pO_2 is defined by the prevalence of certain carriers (defects) [29].

Materials based on CeO_2 and $BaCeO_3$ are oxygen ionic conductors, but along with ionic conductivity under the various pO_2 and pH_2O conditions electron and proton conductivity can appear in them [32–36]. The high values of oxygen ionic conductivity both in fluorite and perovskite are determined by the presence of oxygen vacancies as a result of acceptor doping.

It is typical that when in the oxidizing region oxygen is adsorbed from the gas phase into an anion sublattice site with a formation of electronic holes $h^{\bullet}$ [1,30]:

$$V^{\bullet\bullet}_O + 1/2O_2 \Leftrightarrow^{K_h} O^x_O + 2h^{\bullet}, \quad (2)$$

where K_h is the equilibrium constant of the reaction (2).

Under the reducing conditions a partial desorption of oxygen from crystal lattice takes place, which is accompanied by the reduction of ceria ions from Ce^{4+} (Ce^x_{Ce}) to Ce^{3+} (Ce'_{Ce}) with localized electronic defects appearing [32]:

$$2Ce^x_{Ce} + O^x_O \Leftrightarrow^{K_e} 2Ce'_{Ce} + V^{\bullet\bullet}_O + 1/2O_2, \quad (3)$$

where K_e is the equilibrium constant of reaction (3).

In H_2O-containing atmospheres it is possible that proton defects $OH^{\bullet}_O$ can occur according to [5,30,31]:

$$V^{\bullet\bullet}_O + O^x_O + H_2O \Leftrightarrow^{K_w} 2OH^{\bullet}_O, \quad (4)$$

where K_w is the equilibrium constant of reaction (4).

In fluorite the concentrations of holes and protons are negligible, due to the low values of equilibrium constants K_h and K_w. For example, it was reported [34,35] that the proton conductivity in CeO_2-based materials at 200–800 °C was in the range 10^{-8}–10^{-6} S cm^{-1}. A hole conductivity less than 0.6% of the total was also found in such materials at 750–900 °C [33].

In the range of intermediate and high pO_2 values ($10^{-12} < pO_2$, atm < 1) the total conductivity of $Ce_{0.8}Nd_{0.2}O_{2-\delta}$ is determined by acceptor dopant concentration and equal oxygen ionic conductivity:

$$\sigma_{total} = \sigma_{ion} \approx \text{const}. \quad (5)$$

At low pO_2 ($10^{-23} < pO_2$, atm < 10^{-12}) the total conductivity is defined for both oxygen ionic and electronic charge carriers [34]. The concentration of electronic carriers and, respectively, electron conductivity depends on pO_2 as:

$$\sigma_e \sim \left[Ce'_{Ce}\right] = \left(\frac{K_e}{2}\right)^{1/2} \left[V^{\bullet\bullet}_O\right]^{-1/2} (pO_2)^{-1/4}. \quad (6)$$

At low pO_2 in $BaCeO_3$-based materials the concentration of electronic defects is negligible due to the low value of K_e [25,26,31]. In addition to oxygen ionic conductivity in such

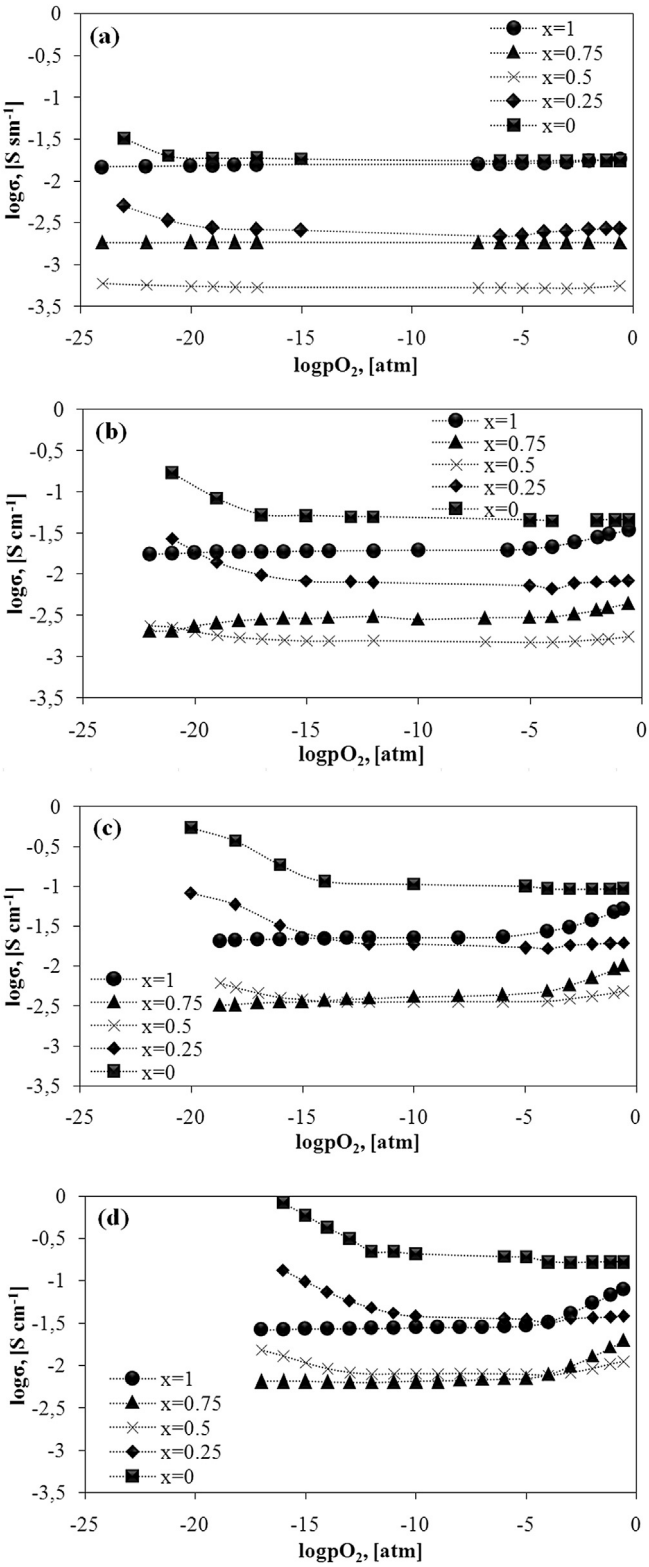

Fig. 6. Oxygen partial pressure dependence of the total conductivity in $(1-x)Ce_{0.8}Nd_{0.2}O_{2-\delta}$–$xBaCe_{0.8}Nd_{0.2}O_{3-\delta}$ samples at 600 °C (a), 700 °C (b), 800 °C (c) and 900 °C (d).

systems a remarkable level of proton conductivity may be obtained in accordance with reaction (4).

Proton conductivity connected with the presence of $[OH_O^{\bullet}]$ defects prevails under wet hydrogen atmosphere in a wide temperature range, or wet ambient (air) atmosphere at relatively low temperatures (less than 700 °C). In $BaCeO_3$-based systems, the concentration of protons decreases with a temperature increase in an oxidizing atmosphere, while the concentration of holes grows.

The pO_2 dependence of the concentration of hole charge carriers and, respectively, hole conductivity at high pO_2 may be written taking into account Eq. (2):

$$\sigma_p \sim p = (K_h)^{1/2}[V_O^{\bullet\bullet}]^{1/2}(pO_2)^{1/4}. \quad (7)$$

Under reducing conditions the conductivity of $BaCeO_3$-based materials is co-ionic and can be defined by the ratio $[V_O^{\bullet\bullet}]/[OH_O^{\bullet}]$, which in turn depends upon the nature of the acceptor dopant, pO_2, pH_2O and the temperature.

Horizontal plateau on the total conductivity dependence in the range of intermediate pO_2 values is determined by a constancy of ionic (oxygen and proton) conductivity, whose value depends only on the amount of acceptor [36]:

$$\sigma_{total} = \sigma_O + \sigma_{OH} \approx \text{const}. \quad (8)$$

A slight decrease in total conductivity in $BaCeO_3$-based systems at low pO_2 is connected with a decrease in proton concentration and an increase in the concentration of oxygen ionic defects due to the dissociation of any residual water vapor present in wet air [37].

Based on the oxygen partial pressure dependence of the total conductivity, shown in Fig. 6, and the defect models proposed above, the following trends can be drawn. When increasing the temperature the electrolytic domain (the area where the ionic conductivity is greater than the electron or hole components of the conductivity) becomes narrower for all the samples. $Ce_{0.8}Nd_{0.2}O_{2-\delta}$ and fluorite-rich composites are characterized by the appearance of electronic conductivity under reducing conditions. In $BaCe_{0.8}Nd_{0.2}O_{3-\delta}$ and composites with a predominance of perovskite phase the noticeable hole conductivity occurs at temperatures above 700 °C. It should be noted that the composite materials possess a lower proportion of the electronic components of total conductivity at high and low pO_2 due to the electron current blocking effect described in our previous work [12], and the studies of Sun et al. [9,38] and Zhu et al. [13].

The effect of concentration on $(1-x)Ce_{0.8}Nd_{0.2}O_{2-\delta}$–$xBaCe_{0.8}Nd_{0.2}O_{3-\delta}$ composite total conductivity, at high (0.21 atm), intermediate (10^{-7} atm) and low (10^{-18} atm) oxygen partial pressure (pO_2) values, was analyzed in comparison with literature data (Fig. 7). As was previously noted, in the oxidizing region (Fig. 7a), a decrease in the conductivity of composite oxides in comparison with basic ones was observed [7,11,39].

The grain size of composites was 1.2–1.7 μm, which is half the grain size reported for $BaCe_{0.8}Nd_{0.2}O_{3-\delta}$ samples (3.7 μm), and four times lower than that reported for $Ce_{0.8}Nd_{0.2}O_{2-\delta}$ (7.8 μm) samples. This is one of the factors which can lead to a decrease in the conductivity of composites. At the same time, with an increase in perovskite content from $x = 0$ to $x = 0.5$ the total resistance of composite materials grows due to not only an increase in both grain and grain boundary resistance of the perovskite phase, but also because of the appearance of an additional component [7]. This component relates to the interfacial resistance which presents a maximum value at $x = 0.5$ due to the very high specific contact area between the grains of different kind and leads to the local minimum in conductivity of the composites at $x = 0.5$, equal to 0.56, 1.75, 4.88 and 11.14 mS cm^{-1} at 600, 700, 800 and 900 °C, respectively. In $(1-x)Ce_{0.8}Sm_{0.2}O_{2-\delta}$–$xBaCe_{0.8}Sm_{0.2}O_{3-\delta}$ [12] and $(1-x)Ce_{0.8}Gd_{0.2}O_{2-\delta}$–$xBaCe_{0.8}Gd_{0.2}O_{3-\delta}$ [8] composites there was no significant decrease observed in conductivity that could be

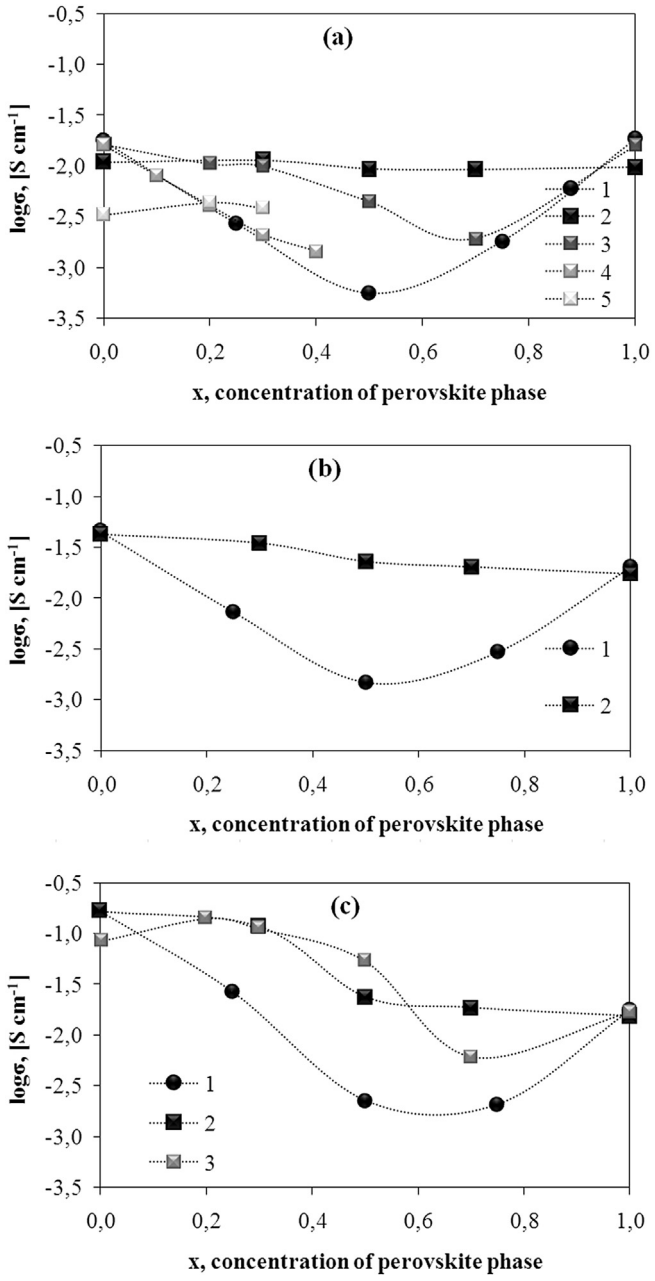

Fig. 7. Concentration dependence of the electrical conductivity for fluorite-perovskite composite systems at: high pO_2 (a), intermediate pO_2 (b) and low pO_2 (c) values. 1) our results at 600 °C (a), 700 °C (b, c); 2) $(1-x)Ce_{0.8}Sm_{0.2}O_{2-\delta}$–$xBaCe_{0.8}Sm_{0.2}O_{3-\delta}$ at 600 °C (a), 750 °C (b, c) [12]; 3) $(1-x)Ce_{0.8}Y_{0.2}O_{2-\delta}$–$xBaCe_{0.7}Zr_{0.1}Y_{0.2}O_{3-\delta}$ (x – wt.%) at 600 °C (a) and 700 °C (c) [11]; 4) $(1-x)Ce_{0.8}Gd_{0.2}O_{2-\delta}$–$xBaCe_{0.8}Gd_{0.2}O_{3-\delta}$ at 600 °C (a) [7]; 5) $(1-x)Ce_{0.8}Gd_{0.2}O_{2-\delta}$–$xBaCe_{0.8}Gd_{0.2}O_{3-\delta}$ at 600 °C (a) [8].

explained by the existence of a weaker influence at the grain boundary and contact resistances in base materials. The analysis of published data [40–42] has conclusively shown that in $Ce_{1-x}Ln_xO_{2-\delta}$ despite the maximal grain conductivity, Nd-doped samples have a grain boundary conductivity (for example, $6.0\cdot10^{-6}$ S cm^{-1} at 350 °C for $x = 0.1$) that is remarkably lower than that in Sm-doped ($4.6\cdot10^{-5}$ S cm^{-1} at 350 °C) and Gd-doped ($8.3\cdot10^{-5}$ S cm^{-1} at 350 °C) samples [42]. In $BaCe_{0.9}Ln_{0.1}O_{3-\delta}$ the conductivity of Nd-doped samples ($1.4\cdot10^{-3}$ S cm^{-1} at 350 °C) is lower than that in Gd- and Sm-doped samples ($4.2\cdot10^{-3}$ S cm^{-1} and $2.0\cdot10^{-3}$ S cm^{-1} at 350 °C, respectively) due to higher grain boundary resistance contribution as well [40].

The concentration dependence of the conductivity in the region of intermediate pO_2 does not differ qualitatively from that obtained at high pO_2 (Fig. 7b). As was noted above, in this region (high pO_2), the conductivity is considered to be ionic. At low pO_2 the conductivity of composites decreases as compared with the one of $Ce_{0.8}Nd_{0.2}O_{2-\delta}$ (Fig. 7c). This behavior is attributed to both the decrease in the ionic conductivity when increasing perovskite phase content, and partial blocking of electronic charge carriers by perovskite phase as was mentioned earlier.

From experimental data the partial contributions of ionic, electronic and hole conductivities were calculated according to the known empirical equation [27,43,44]:

$$\sigma_{total} = \sigma_{e,o}\cdot(pO_2)^{-1/4} + \sigma_{ion,o} + \sigma_{p,o}\cdot(pO_2)^{1/4}, \quad (9)$$

where $\sigma_{e,o}$, $\sigma_{p,o}$ are electronic and hole conductivity at $pO_2 = 1$ atm, $\sigma_{ion,o}$ is the sum of oxygen ionic and proton conductivity (which were considered approximately constants). The partial

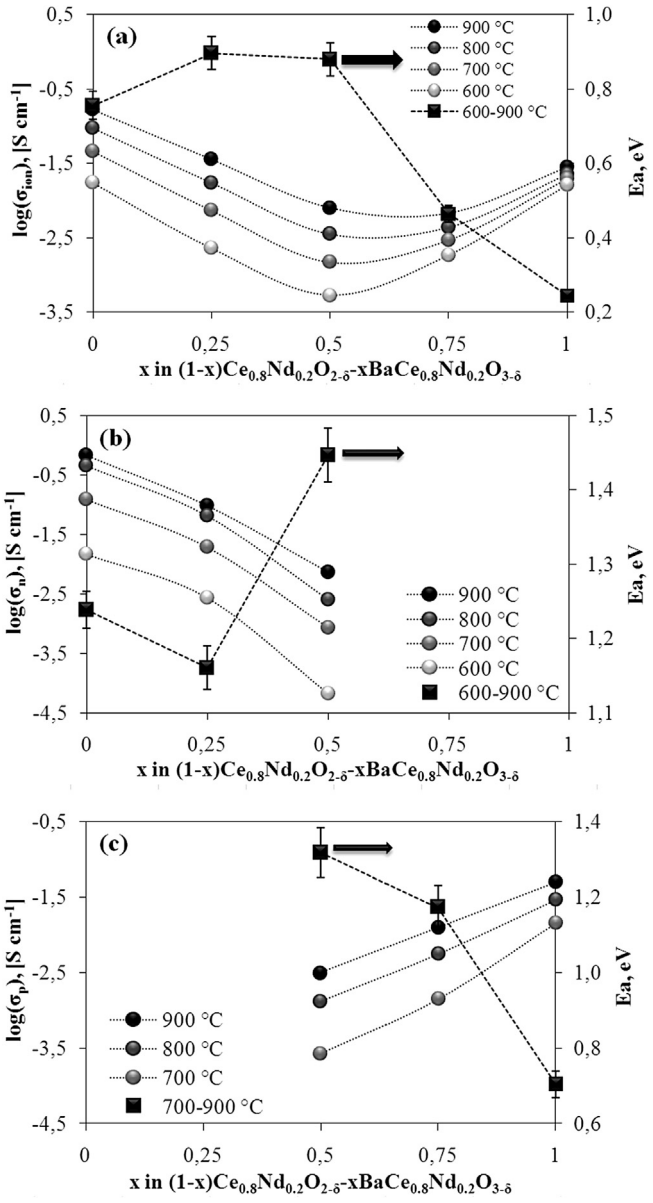

Fig. 8. Concentration dependence of the ionic (a), electronic (b) and hole (c) conductivity of $(1-x)Ce_{0.8}Nd_{0.2}O_{2-\delta}$–$xBaCe_{0.8}Nd_{0.2}O_{3-\delta}$ ceramic samples with corresponding value of activation energy.

conductivities obtained from the combination of the experimental data and Eq. (9) should be considered as effective values, which do not refer to the component that determines the transport nature of system, but two-phased composite in a whole. The concentration dependences of partial conductivities and calculated activation energy are presented in Fig. 8.

The concentration dependence of the ionic conductivity at 600–900 °C (Fig. 8a) corresponds to the data presented above at 700 °C (Fig. 8b) and retains a similar trend at other temperatures. Comparison of E_a of the ionic conductivity with those of the total conductivity indicates that both base systems and composite materials possess predominantly ionic conductivity.

The electronic conductivity decreases with an increase of perovskite phase content as depicted in Fig. 8b, and at $x = 0.75$ and in $BaCe_{0.8}Nd_{0.2}O_{3-\delta}$ ($x = 1$) does not exceed 5% of the total conductivity. Conversely, hole conductivity, as observed in $(1-x)Ce_{0.8}Nd_{0.2}O_{2-\delta}$–$xBaCe_{0.8}Nd_{0.2}O_{3-\delta}$ ($0.5 \le x \le 1$), grows with x (Fig. 8c). The activation energy of the electron and hole conductivity in two-phase materials is higher than that in $Ce_{0.8}Nd_{0.2}O_{2-\delta}$ and $BaCe_{0.8}Nd_{0.2}O_{3-\delta}$, which confirms the blocking phenomenon of both the electron and hole conductivity in composites. The values of activation energy of partial conductivities are consistent with literature data for materials based on cerium oxide [16,45] and barium cerate [5,26,28].

3.4. Electrical conductivity during redox-cycling

In Fig. 9 the results of the stability investigation of the electrical properties of $(1-x)Ce_{0.8}Nd_{0.2}O_{2-\delta}$–$xBaCe_{0.8}Nd_{0.2}O_{3-\delta}$ ceramic samples at 900 °C are presented. It was found that after 2 redox cycles the conductivity in $Ce_{0.8}Nd_{0.2}O_{2-\delta}$ decreases by 85%. This can be connected with changes of the oxidation state of ceria, accompanied by expansion/compression of the fluorite lattice, and leads to the mechanical instability of ceramics and volume destruction of the samples, which may be the reason for the appearance of cracks (Fig. 10a) and such a dramatic fall in conductivity. The conductivity of $BaCe_{0.8}Nd_{0.2}O_{3-\delta}$ decreases by 30% from an initial value. Perhaps this is due to the localization of the different types of point defects at the grain boundaries. After several redox cycles increased defects concentration and their interaction leads to the formation of three-dimensional defects (micro-cracks) along the grain boundaries (Fig. 10e). The resulting degradation of the composite materials in terms of the conductivity is no more than 15%. The surface of composites is characterized by only local pores on the surfaces of the composites, which do not have a significant influence on their electrical properties (Fig. 10b–d).

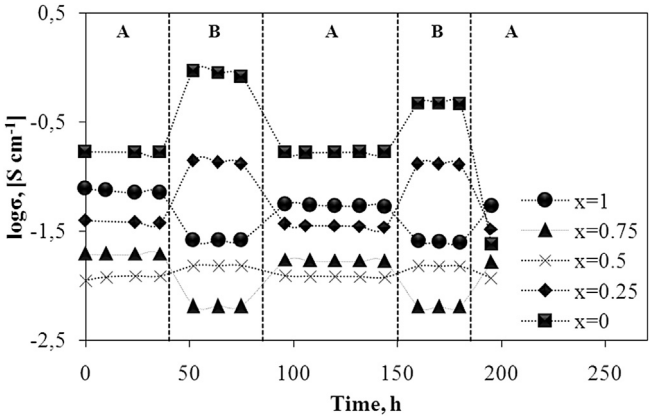

Fig. 9. The effect of time on the $(1-x)Ce_{0.8}Nd_{0.2}O_{2-\delta}$–$xBaCe_{0.8}Nd_{0.2}O_{3-\delta}$ conductivity at 900 °C. A corresponds to $pO_2 = 0.21$ atm, whereas B to $pO_2 = 1 \cdot 10^{-18}$ atm.

3.5. Chemical and thermal expansion

To confirm the possible impact of changes in the lattice parameters and consequently the geometric size of ceramics in the oxidation/reduction cycling, the isothermal (chemical) expansion of both the basic materials and the composite with an equimolar content of the phases was measured (Fig. 11). For CeO_2-based ceramics ($x = 0$) a steep increase in linear dimensions (by 0.38%) was observed at the change of pO_2 value from $1 \cdot 10^{-15}$ to $1 \cdot 10^{-18}$ atm, which indicated the reaction had occurred (3) and the partial reduction of Ce^{4+}-ions ($r_{Ce^{4+}_{VIII}} = 0.970$ Å) to Ce^{3+}-ions ($r_{Ce^{3+}_{VIII}} = 1.143$ Å) [46]. A similar trend was noted earlier by Gorelov et al. [47]. The authors reported a change in the linear dimensions of 0.05, 0.15 and 0.27% at 600, 700 and 800 °C, respectively in $Ce_{0.8}Gd_{0.2}O_{2-\delta}$ electrolyte in the range of $1 \cdot 10^{-25} \le pO_2$, atm$\le 1 \cdot 10^{-8}$.

For $BaCeO_3$-based ceramics ($x = 1$) a slight decrease in the linear dimensions at $pO_2 < 1 \cdot 10^{-15}$ atm was observed. Recall that the oxygen pumping is conducted from the ambient air, which contains a small amount of gaseous water. Thus, in this range the residual dissociation of water vapor [37] occurred, which reduces the number of proton defects in the oxide (reverse reaction of reaction (4)) and, correspondingly, decreases the cell parameters and linear dimensions of the ceramic.

For the composite material ($x = 0.5$) a slight increase in the linear dimensions of the sample in the reduction area was observed. This did not exceed 0.03% relative to the initial ones in an oxidizing atmosphere. These data confirm that the cracks which appeared in $Ce_{0.8}Nd_{0.2}O_{2-\delta}$ (Fig. 10a) are the result of a significant variation in the lattice parameters in the process of redox cycles.

Consequently, the use of CeO_2- and $BaCeO_3$-based ceramics is to be expected at intermediate temperatures (IT-SOFC). However, conductivity and chemical expansion data obtained under redox cycles at 900 °C permits comparative assessment on the degree and depth of degradation in the $(1-x)Ce_{0.8}Nd_{0.2}O_{2-\delta}$–$xBaCe_{0.8}Nd_{0.2}O_{3-\delta}$ system, and to extend these results to lower temperatures. From this viewpoint, the composite ceramics are characterized by minor fluctuations in the dimensions of the sample passing from the oxidation atmosphere to the reduction (or vice versa), and relatively superior stability is present in an atmosphere containing CO_2 and H_2O components [12].

Finally, the thermal expansion of $(1-x)Ce_{0.8}Nd_{0.2}O_{2-\delta}$–$xBaCe_{0.8}Nd_{0.2}O_{3-\delta}$ ceramic samples was investigated in the temperature range of 25–880 °C in a wet air atmosphere (Fig. 12a). The graph shows that the temperature dependence of the expansion for $Ce_{0.8}Nd_{0.2}O_{2-\delta}$ was not characterized by a sharp change in linear dimensions unlike other curves. For $BaCe_{0.8}Nd_{0.2}O_{3-\delta}$ and composites the change in the slope is observed, which may be associated with a change of the perovskite structure symmetry. A similar trend is noted in our recent work for Sm-doped CeO_2–$BaCeO_3$ [12].

It should be noted that the temperature of the slope change (was calculated on the base of maximum difference of experimental data and linear fitting) is not constant and increases when increasing perovskite phase: for samples with $x = 0.25$, 0.5, 0.75 and 1 the temperature of break point (T^*) is equal to 460, 480, 500 and 510 °C, respectively. For $Ce_{0.8}Nd_{0.2}O_{2-\delta}$ the thermal expansion coefficient (TEC) value calculated in the whole temperature range is equal $10.9 \cdot 10^{-6}$ K^{-1}. For composite materials and $BaCe_{0.8}Nd_{0.2}O_{3-\delta}$ TEC was calculated for two temperature intervals (Fig. 12b). It is clear that for low temperature range (20–T^* °C) the decrease of TEC from $8.7 \cdot 10^{-6}$ to $8.2 \cdot 10^{-6}$ K^{-1} is observed for $x = 0$, $x = 0.25$ and 1, respectively, whereas for high temperature range (T^*–880 °C) the reverse tendency is realized (from $11.1 \cdot 10^{-6}$

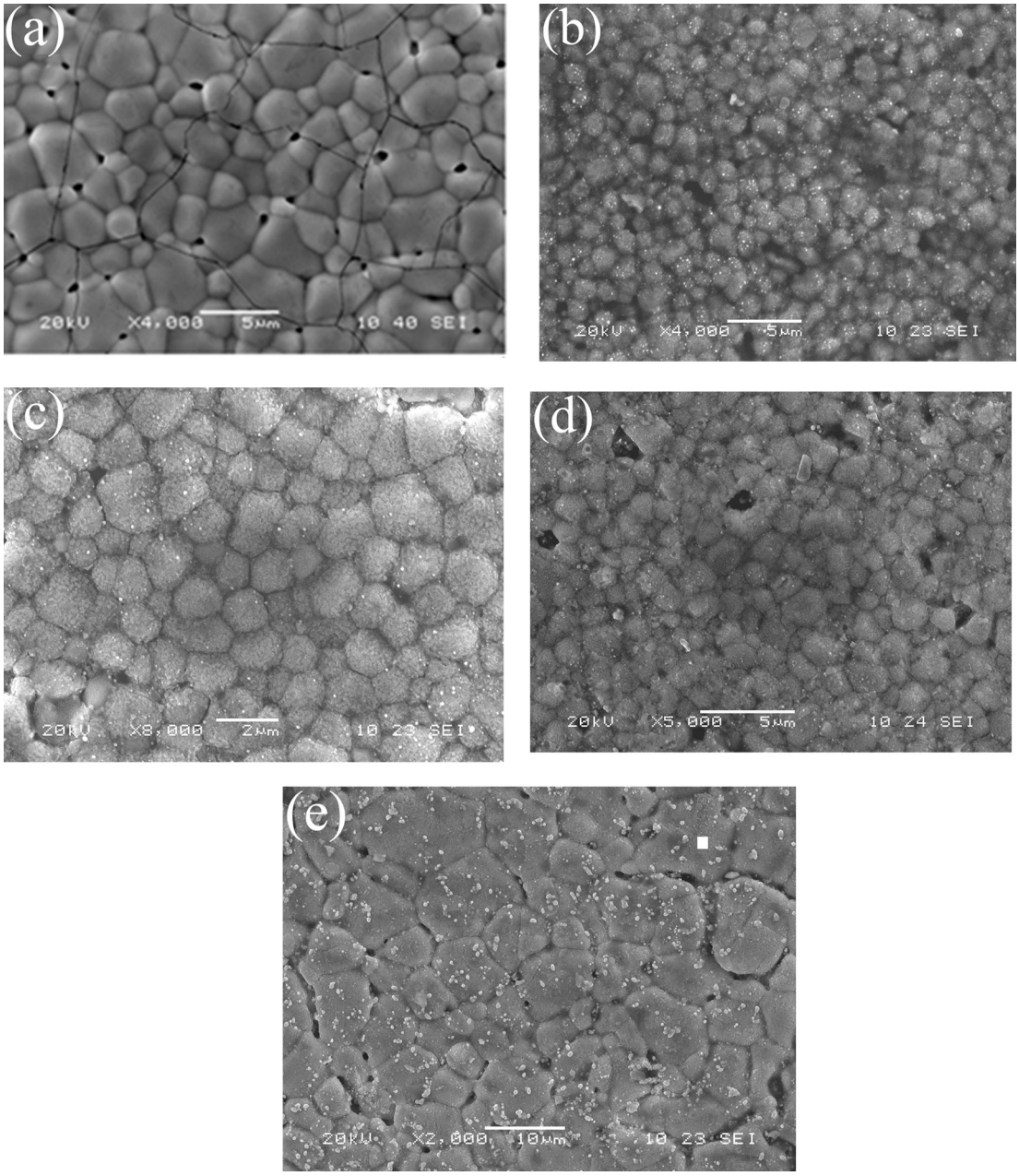

Fig. 10. SEM micrographs of $(1-x)Ce_{0.8}Nd_{0.2}O_{2-\delta}$– $xBaCe_{0.8}Nd_{0.2}O_{3-\delta}$ samples after redox measurements: $x = 0$ (a), $x = 0.25$ (b), $x = 0.5$ (c), $x = 0.75$ (d) and $x = 1$ (e).

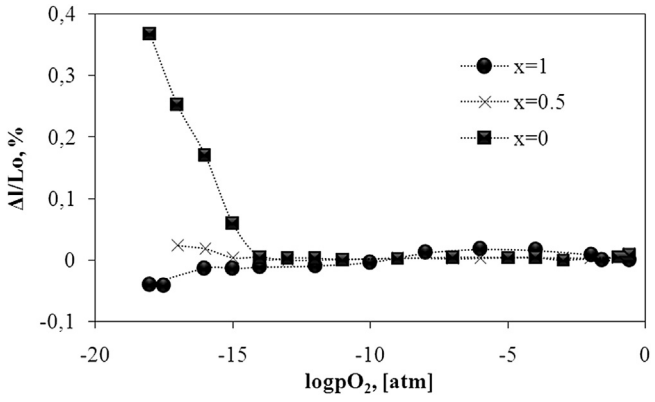

Fig. 11. Oxygen partial pressure dependence of the isothermal expansion in $(1 - x)Ce_{0.8}Nd_{0.2}O_{2-\delta}$–$xBaCe_{0.8}Nd_{0.2}O_{3-\delta}$ samples at 900 °C.

to $14.0 \cdot 10^{-6}$ K^{-1} for $x = 0.25$ and 1, respectively). These TEC values are close to those reported for known IT-SOFC's electrolytes [48].

4. Conclusions

In the present work nano-sized powders of $(1-x)Ce_{0.8}Nd_{0.2}O_{2-\delta}$–$xBaCe_{0.8}Nd_{0.2}O_{3-\delta}$ were prepared by employing the one-step citrate-nitrate combustion method using citric acid as a fuel. It was determined that the phase structure of the individual oxides $Ce_{0.8}Nd_{0.2}O_{2-\delta}$ and $BaCe_{0.8}Nd_{0.2}O_{3-\delta}$ corresponds to the fluorite and perovskite structure, respectively. The composite materials of $(1 - x)Ce_{0.8}Nd_{0.2}O_{2-\delta}$–$xBaCe_{0.8}Nd_{0.2}O_{3-\delta}$ consist of two phases with the same structures without any traces of other impurities. The corresponding well-densified ceramic materials were obtained during sintering at 1500 °C for 3 h. The mean grain size of composite materials did not differ significantly, and varied from 1.2 to 1.7 μm, whereas for $Ce_{0.8}Nd_{0.2}O_{2-\delta}$ and

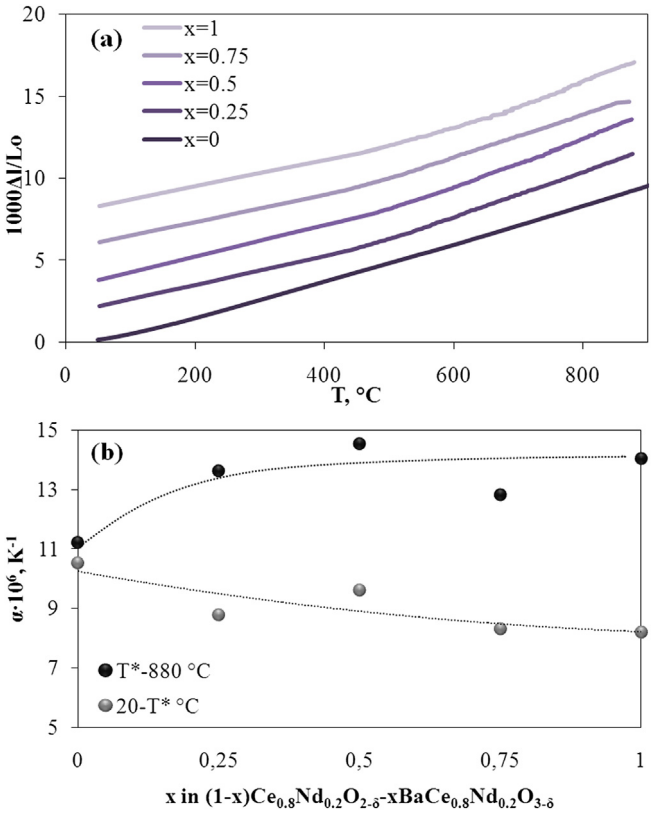

Fig. 12. Thermal expansion behavior of $(1-x)Ce_{0.8}Nd_{0.2}O_{2-\delta}$–$xBaCe_{0.8}Nd_{0.2}O_{3-\delta}$ ceramics: (a) in wet air atmosphere and (b) concentration dependences of TEC in low- and high temperature range.

$BaCe_{0.8}Nd_{0.2}O_{3-\delta}$ materials the grain size was 3.7 and 7.8 μm, respectively.

The influence of the phase content on the nature of conductivity and thermal properties of $(1-x)Ce_{0.8}Nd_{0.2}O_{2-\delta}$–$xBaCe_{0.8}Nd_{0.2}O_{3-\delta}$ is examined. The total conductivity of the novel composite materials in wet air is lower than that of the basic oxides. This is connected with the high contact resistance of the boundaries between two different phases, leading to an increase of the activation energy of the total conductivity, with the activation energy maximum and the conductivity minimum found in $0.5Ce_{0.8}Nd_{0.2}O_{2-\delta}$–$0.5BaCe_{0.8}Nd_{0.2}O_{3-\delta}$. In the sample with x = 0.25 the conductivity is primarily controlled by the fluorite phase, whereas in composites with $x = 0.5$ and 0.75, transport is apparently controlled by the perovskite phase.

The concentration dependence of total conductivity in $(1-x)Ce_{0.8}Nd_{0.2}O_{2-\delta}$–$xBaCe_{0.8}Nd_{0.2}O_{3-\delta}$ composite at high (0.21 atm), intermediate (10^{-7} atm) and low (10^{-18} atm) pO_2 values was analyzed: In the oxidizing region, a decrease in conductivity of composite oxides in comparison with the basic ones was observed. In the region of intermediate pO_2 the conductivity was similar to that obtained at high pO_2 and considered to be ionic. At low pO_2 the conductivity decreases and this behavior is attributed to both the decrease in ionic conductivity when increasing perovskite phase content, and the partial blocking of electronic charge carriers by perovskite phase.

Additionally, the degradation of $(1-x)Ce_{0.8}Nd_{0.2}O_{2-\delta}$–$BaCe_{0.8}Nd_{0.2}O_{3-\delta}$ materials was investigated at 900 °C (for 200 h) under dynamically changed atmospheric conditions (redox-cycles), and the stability of electrical properties was discussed using the SEM data and chemical expansion results. The conductivity in $Ce_{0.8}Nd_{0.2}O_{2-\delta}$ decreased by 85%, whereas the conductivity in $BaCe_{0.8}Nd_{0.2}O_{3-\delta}$ decreased by 30% after 2 redox cycles. The resulting degradation of the $(1-x)Ce_{0.8}Nd_{0.2}O_{2-\delta}$–$xBaCe_{0.8}Nd_{0.2}O_{3-\delta}$ composite in terms of the conductivity was no more than 15%. The relatively superior stability of the novel Nd-doped perovskite-fluorite composites in an atmosphere containing CO_2 and H_2O components may render them as potential candidates to be employed in IT-SOFCs.

Acknowledgments

The present work was financially supported by the Council of the President of the Russian Federation (grants № СП-44.2012.1), the Russian Foundation for Basic Research and the Government of Sverdlovsk Region (grants № 13-03-00065, 13-03-96098). Prof. P. Tsiakaras is grateful to the Greek Ministry of Development-GSRT "SYNERGASIA" Program (09SYN-32-615: ECHOCO2) for the financial support.

The authors are also grateful to the Shared Access Center "Composition of Compounds" of the Institute of High Temperature Electrochemistry for the attestation of powder and ceramic materials.

References

[1] F.M.L. Figueiredo, F.M.B. Marques, WIREs Energy Environ. 2 (2013) 52–72.
[2] A. Orera, P.R. Slater, Chem. Mater. 22 (2010) 675–690.
[3] A.J. Jacobson, Chem. Mater. 22 (2010) 660–674.
[4] N.H. Menzler, F. Tietz, S. Uhlenbruck, H.P. Buchkremer, D. Stöver, J. Mater. Sci. 45 (2010) 3109–3135.
[5] K.D. Kreuer, Annu. Rev. Mater. Res. 33 (2003) 333–359.
[6] E. Fabbri, D. Pergolesi, E. Traversa, Chem. Soc. Rev. 39 (2010) 4355–4369.
[7] A. Venkatasubramanian, P. Gopalan, T.R.S. Prasanna, Int. J. Hydrogen Energy 35 (2010) 4597–4605.
[8] M. Khandelwal, A. Venkatasubramanian, T.R.S. Prasanna, P. Gopalan, J. Eur. Ceram. Soc. 31 (2011) 559–568.
[9] W. Sun, Y. Jiang, Y. Wang, S. Fang, Z. Zhu, W. Liu, J. Power Sources 196 (2011) 62–68.
[10] D. Lin, Q. Wang, K. Peng, L.L. Shaw, J. Power Sources 205 (2012) 100–107.
[11] J. Huang, L. Zhang, C. Wang, P. Zhang, Int. J. Hydrogen Energy 37 (2012) 13044–13052.
[12] D. Medvedev, V. Maragou, E. Pikalova, A. Demin, P. Tsiakaras, J. Power Sources 221 (2013) 217–227.
[13] B. Zhu, X. Liu, T. Schober, Electrochem. Commun. 6 (2004) 378–383.
[14] N.V. Sharova, V.P. Gorelov, Russ. J. Electrochem. 41 (2005) 1001–1007.
[15] N.V. Sharova, V.P. Gorelov, Russ. J. Electrochem. 40 (2004) 639–645.
[16] E.Yu. Pikalova, A.A. Murashkina, V.I. Maragou, A.K. Demin, V.N. Strekalovsky, P.E. Tsiakaras, Int. J. Hydrogen Energy 36 (2011) 6175–6183.
[17] L. Li, X. Lin, G. Li, H. Inomata, J. Mater. Res. 16 (2001) 3207–3213.
[18] L. Li, R. Kasse, S. Phadke, W. Qiu, A. Hug, J.C. Nino, Solid State Ionics 221 (2012) 15–21.
[19] W. Chen, F. Li, J. Yu, J. Mater. Lett. 60 (2006) 57–60.
[20] D.A. Medvedev, E.Yu. Pikalova, A.K. Demin, V.R. Khrustov, I.V. Nikolaenko, A.V. Nikonov, V.B. Malkov, B.D. Antonov, Russ. J. Phys. Chem. A 87 (2) (2013) 270–277.
[21] http://zirconiaproject.wordpress.com/devices/zirconia-318/.
[22] M.R. Kosinski, R.T. Baker, J. Power Sources 196 (2011) 2498–2512.
[23] Y.-C. Lee, I.-M. Hung, S.-L. Chang, C.-J. Ciou, J.-S. Wu, J. Eur. Ceram. Soc. 31 (2011) 3137–3143.
[24] X.-M. Lin, L.-P. Li, G.-S. Li, W.-H. Su, Mater. Chem. Phys. 69 (2001) 236–240.
[25] N.V. Sharova, V.P. Gorelov, V.B. Balakireva, Russ. J. Electrochem. 41 (2005) 665–670.
[26] D.-K. Lim, C.-J. Park, M.-B. Choi, C.-N. Park, S.-J. Song, Int. J. Hydrogen Energy 35 (2010) 10624–10629.
[27] N. Bonanos, F.W. Poulsen, J. Mater. Chem. 9 (1999) 431–434.
[28] D.-K. Lim, H.-N. Im, S.-Y. Jeon, J.-Y. Park, S.-J. Song, Acta Mater. 61 (2013) 1274–1283.
[29] Kröger FA. The Chemistry of Imperfect Crystals. Amsterdam: North-Holland Publishing Co..; 1964.
[30] N. Bonanos, Solid State Ionics 145 (2001) 265–274.
[31] S.-J. Song, E.D. Wachsman, S.E. Dorris, U. Balachandran, Solid State Ionics 149 (2002) 1–10.
[32] D. Pérez-Coll, D. Marrero-López, J.C. Ruiz-Morales, P. Núñez, J.C.C. Abrantes, J.R. Frade, J. Power Sources 173 (2007) 291–297.
[33] D. Pérez-Coll, P. Núñez, J.R. Frade, J. Power Sources 227 (2013) 145–152.
[34] Y. Nigara, K. Yashiro, T. Kawada, J. Mizusaki, Solid State Ionics 159 (2003) 135–141.
[35] E. Ruiz-Trejo, J.A. Kilner, J. Appl. Electrochem. 39 (2009) 523–528.

[36] A.V. Kuz'min, V.B. Balakireva, S.V. Plaksin, V.P. Gorelov, Russ. J. Electrochem. 45 (2009) 1351–1357.
[37] D.A. Medvedev, E.V. Gorbova, A.K. Demin, B.D. Antonov, Russ. J. Electrochem. 47 (2011) 1404–1410.
[38] W. Sun, W. Liu, J. Power Sources 217 (2012) 114–119.
[39] C.-W. Nan, Prog. Mater. Sci. 37 (1993) 1–116.
[40] M. Amsif, D. Marrero-Lopez, J.C. Ruiz-Morales, S.N. Savvin, M. Gabás, P. Núñez, J. Power Sources 196 (2011) 3461–3469.
[41] W. Zając, J. Molenda, Solid State Ionics 179 (2008) 154–158.
[42] N. Chaubey, B.N. Wani, S.R. Bharadwaj, M.C. Chattopadhyaya, Solid State Sci. 20 (2013) 135–141.
[43] U.N. Shrivastava, K.L. Duncan, J.N. Chung, Int. J. Hydrogen Energy 37 (2012) 15350–15358.
[44] M. Oishi, S. Akoshima, K. Yashiro, K. Sato, J. Mizusaki, T. Kawada, Solid State Ionics 179 (2008) 2240–2247.
[45] E.Yu. Pikalova, V.I. Maragou, A.N. Demina, A.K. Demin, P.E. Tsiakaras, J. Power Sources 181 (2008) 199–206.
[46] R.D. Shannon, Acta Crystallogr. A 32 (1976) 751–767.
[47] V.P. Gorelov, V.B. Balakireva, I.Yu. Yaroslavtsev, V.A. Kazantsev, E.G. Vaganov, Russ. J. Electrochem. 43 (2007) 888–893.
[48] D. Medvedev, A. Murashkina, E. Pikalova, A. Demin, A. Podias, P. Tsiakaras, Prog. Mater. Sci. 60 (2014) 72–129.